

Robinson, Nucl. Phys. **A132**, 593 (1969).

³⁰R. J. Blin-Stoyle and J. M. Freeman, Nucl. Phys. **A150**, 369 (1970).

³¹H. Bühring and H. Schopper, Kernforschungszentrum, Karlsruhe Report No. KFK-307, 1965 (unpublished).

³²V. V. Vladimirsky, V. K. Grigorev, V. A. Ergakov,

D. P. Zharkov, and Y. V. Trebukhovsky, Izv. Akad. Nauk SSSR, Ser. Fiz. **25**, 1121 (1961) [Bull. Acad. Sci. U.S.S.R., Phys. Ser. **25**, 1128 (1961)].

³³C. J. Christensen, V. E. Krohn, and G. R. Ringo, Phys. Rev. C **1**, 1693 (1970).

PHYSICAL REVIEW D

VOLUME 5, NUMBER 7

1 APRIL 1972

Total Hadronic Cross Section of γ Rays in Hydrogen in the Energy Range 0.265–4.215 GeV

T. A. Armstrong, W. R. Hogg, G. M. Lewis, and A. W. Robertson
Department of Natural Philosophy, The University, Glasgow, Scotland

and

G. R. Brookes, A. S. Clough,* J. H. Freeland, W. Galbraith, and A. F. King
Department of Physics, The University, Sheffield, Yorkshire, England

and

W. R. Rawlinson, N. R. S. Tait, J. C. Thompson, and D. W. L. Tolfree
Daresbury Nuclear Physics Laboratory, Daresbury, Cheshire, England

(Received 30 November 1971)

The total cross section of γ rays in hydrogen resulting in hadron production, σ_T , has been measured over the energy range 265–4215 MeV. A tagging system with narrow energy bins was employed. Structure in the resonance region followed by a steady fall with energy has been observed and the results are analyzed. The forward amplitude of γ -proton scattering is evaluated, and its behavior in the Argand diagram studied as a function of energy. The relationships of the measurements to Regge-pole theory and the vector-dominance model are detailed.

I. INTRODUCTION

Total cross sections for long-lived strongly interacting particles can generally be determined by absorption methods. Good data on these, over a wide energy band, have therefore been accumulating for some time.

A measurement of the total cross section for γ rays, σ_T , involving strong-interaction vertices has, however, to be made in a different way because this γ -ray cross section is dwarfed by those of the prolific purely electromagnetic processes. Also γ rays are generally available, at high energies, only as the broad and steeply changing bremsstrahlung spectrum, making monochromatic studies very difficult.

At the time this experiment was started little direct data existed as a function of energy. Recourse had generally to be made to a compilation of the separate processes where known, the contribution of each being roughly assessed from often sparse differential cross-section data. Ad-

ditional information came from bubble-chamber work, particularly that using monochromatic beams.¹

Quite recently the situation has changed in a number of ways. A study of inelastic electron scattering at SLAC,² for various squared four-momentum transfers q^2 of the virtual photon, led to an extrapolation to $q^2=0$, providing an indirect assessment of σ_T for real photons. Direct measurements of σ_T have now also been reported, in several energy bands.

These direct investigations measure the production rates of hadronic events, and successfully reject the vastly preponderant electromagnetic events by an angular separation. The use of a tagging system enables the energy of the incident γ ray responsible for an observed hadronic event to be identified. As compensation for the trouble of setting up such a system the bremsstrahlung spectrum can be then turned to good use; it enables the energy dependence of σ_T to be displayed over a wide range of energy values in a single experimental run.

Work in the higher-energy regions using tagging systems with fairly wide energy bins (~ 100 MeV and greater) has been reported on by DESY³ and SLAC.⁴ We have reported preliminary data on the γ -ray excitation of the various baryon resonances in the energy range 265 to 1840 MeV, using narrow energy bins.^{5(a)} We have now carried out further measurement work in the resonance region and up to 4.215 GeV for hydrogen and deuterium, at the Daresbury Nuclear Physics Laboratory. A brief account of some results was submitted to the Cornell Symposium.^{5(b)} Detailed results for hydrogen are reported below.

II. THEORETICAL CONSIDERATIONS

The study of the total γ -ray-proton cross section, σ_T , is closely linked to proton Compton scattering. The forward scattering amplitude $F(\nu)$, of a photon of energy ν in the laboratory frame, is of the operator form⁶:

$$F(\nu) = f_1(\nu) \vec{\epsilon}' \cdot \vec{\epsilon} + if_2(\nu) \vec{\sigma} \cdot \vec{\epsilon}' \times \vec{\epsilon}. \quad (1)$$

Here $\vec{\epsilon}$ and $\vec{\epsilon}'$ are the initial and final photon polarization vectors, and $\vec{\sigma}$ is the proton spin operator. Thus only $f_1(\nu)$ occurs in the proton spin-averaged forward amplitude. Consequently $\text{Im}f_1$ is expressible in terms of σ_T , the spin-averaged total cross section, by the optical theorem.

Explicitly by this theorem, and using dispersion relations to evaluate $\text{Re}f_1(\nu)$,⁷

$$f_1(\nu) = f_1(0) + \frac{\nu^2}{2\pi^2} P \int_{\nu_0}^{\infty} \frac{\sigma_T d\nu'}{\nu'^2 - \nu^2} + \frac{i\nu}{4\pi} \sigma_T. \quad (2a)$$

Here

$$f_1(0) = -e^2/M, \quad (2b)$$

the Thomson amplitude as $\nu \rightarrow 0$, M being the proton mass. Numerically $f_1(0) = -3.0 \mu\text{b GeV}$, and ν_0 is the threshold energy for pion photoproduction.

Once a smooth fit to the experimental curve for σ_T has been obtained, the phase characteristics of the scattering amplitude $f_1(\nu)$ can be evaluated, in a manner similar to that used by Damashek and Gilman.⁷ In particular, a detailed examination can then be made of the plot of the scattering amplitude, in an Argand diagram, as a function of the center-of-mass energy. In this over-all way a detailed analysis can be made of the presence of, and the contributions of the various possible excited baryon states, N , Δ , produced in γ - p scattering and photoproduction.

Comparisons can furthermore be made between σ_T data and available data on the forward scattering of γ rays. For unpolarized targets, and beams, the forward differential γ -scattering cross section in laboratory coordinates can be written:

$$\left(\frac{d\sigma}{d\Omega}\right)_{\theta=0} = |f_1(\nu)|^2 + |f_2(\nu)|^2. \quad (3)$$

This scattering is small and difficult to measure at high energies, e.g., for γ rays of 1 GeV, $(d\sigma/d\Omega)_{\theta=0}$ is near to $1 \mu\text{b/sr}$. On the other hand, at this energy, the hadronic cross section proves to be around $230 \mu\text{b}$. So, as far as the contribution $|f_1|^2$ is concerned, an accurate assessment can be obtained from the σ_T data, via Eq. (2). In this sense σ_T data provide a magnified image of f_1 . The quantity f_2 is believed to be small.⁸

The high-energy behavior of σ_T (extrapolated or assumed) and of $f_1(\nu)$ enters into the detailed evaluations of Eq. (2). Photon scattering at the highest energies is associated with the effects of the Pommeranchuk pole in the $p\bar{p} \rightarrow \gamma\gamma$ cross channel to provide an asymptotic constant total cross section. At energies of a few GeV, fits are usually made with the aid of additional $\alpha(0) = 0.5$ Regge trajectories, i.e., with a relation of form⁷

$$\sigma_T(\nu) = a_1 + a_2/\nu^{1/2}. \quad (4)$$

Recently, however, it has been shown possible to derive information on the precise form of assumed Regge-pole contributions at high energy, on the sole basis of low-energy data, using the continuous-moment sum rules.⁹ In this sense σ_T data over a limited range, say from pion photoproduction threshold to 4 GeV, are adequate for the evaluation of both real and imaginary parts of $f_1(\nu)$ over the whole energy range.

It has been suggested that the forward scattering amplitude $f_1(\nu)$ might simulate an expression⁷ of an extended Regge type, denoted $f_1^R(\nu)$:

$$f_1^R(\nu) = C - \sum_j \frac{a_j}{4\pi} \frac{1 + e^{-i\pi\alpha_j(0)}}{\sin\pi\alpha_j(0)} \nu^{\alpha_j(0)} \quad (5a)$$

as $\nu \rightarrow \infty$. Here attention is normally restricted to the Pommeranchukon trajectory $\alpha_1(0) = 1$ and the neighboring Regge trajectory $\alpha_2(0) = 0.5$. Interest also centers on the possible existence of a real constant C which might be interpreted as a fixed pole. This leads to an effective sum rule⁷:

$$C = f_1(0) - \frac{2}{\pi} \int_{\nu_0}^N \frac{d\nu'}{\nu'} \text{Im}f_1(\nu') + \frac{2}{\pi} \int_{\nu_0}^N \frac{d\nu'}{\nu'} \text{Im}f_1^R(\nu'), \quad (5b)$$

where N is high enough to suppose $\text{Im}f_1(\nu) = \text{Im}f_1^R(\nu)$ valid for $\nu \geq N$. Explicitly Eq. (5b) then gives

$$C = -3.0 - \frac{1}{2\pi^2} \int_{\nu_0}^N \sigma_T(\nu') d\nu' + \frac{N}{2\pi^2} \left(a_1 + \frac{2a_2}{N^{1/2}} \right) \quad (5c)$$

in $\mu\text{b GeV}$.

Lastly, at the higher energies the photon with its spin of 1 can be expected to be increasingly capable of simulating the behavior of the various vector mesons. In this way the total cross section σ_T can be evaluated in terms of hadronic interactions

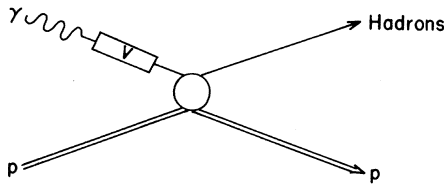


FIG. 1. The vector-dominance model.

(Fig. 1). Specifically $\sigma_T(\gamma p)$ will be related to the succession $\sigma_T(Vp)$ through the coupling constants $1/\gamma_V$, i.e.,

$$\sigma_T(\gamma p) = \alpha\pi \sum_{V=\rho, \omega, \phi} \frac{1}{\gamma_V^2} \sigma_T(Vp). \quad (6)$$

The quantities γ_V can be inferred from the leptonic decay of a ρ meson or from storage-ring experiments. Using the quark model for linking the vector-meson cross sections $\sigma_T(Vp)$ with the pseudoscalar-meson cross sections $\sigma_T(\pi p)$ and $\sigma_T(Kp)$, Joos¹⁰ predicted a value of $\sigma_T(\gamma p)$ at 6 GeV of $106 \mu\text{b}$.

III. EXPERIMENTAL METHOD

A. Experimental Arrangement

The angular distributions of purely electromagnetic events and hadronic photoproduced events are very different. The former are concentrated forwards. Thus at least one product of the Compton electron and triplet processes is emitted within an angle of $\theta_1 = (2\mu/\nu)^{1/2}$ to the beam direction, where μ is the electron mass, e.g., within $\pm 1.75^\circ$ for 1-GeV γ rays. For pair production, the probability of finding both members outside an angle θ_2 falls off somewhat more rapidly than $1/\nu^2\theta_2^2$. For $\theta_2 = \pm 3.5^\circ$ for instance, little more than a microbarn would be contributed for the lowest-energy γ rays studied here. For hadronic interactions emission could be generally expected to be well outside these angles. Bubble-chamber data¹¹ indicate that the yields of hadronic events within such angles would be at most a few percent. Moreover, corrections

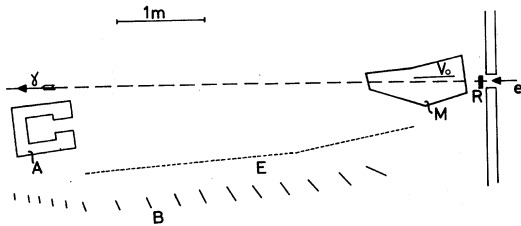


FIG. 2. Illustration of the tagging system. A weak electron beam strikes a radiator R . Tagging of γ rays produced is effected by the 64 electron counters E , associated in groups of four, with the backing counters B .

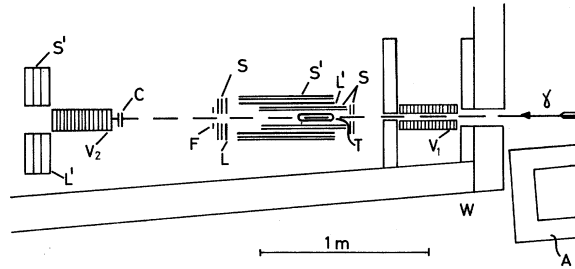


FIG. 3. Schematic diagram of the detection system. The γ rays pass through the hole in the collimator veto counter V_1 to interact in the liquid-hydrogen cell T , 200 mm long and 44 mm in diameter. Hadronic events are detected in the surrounding box of paired scintillators S , and π^0 counters S' . L and L' denote lead converters. Forward-going electromagnetic events are vetoed by the shower counter V_2 , and electron counters C . A coincidence between a hadron counter and a tagging counter constitutes an event, and the channel number of the tagging counter is recorded on tape.

for these can be accurately assessed in a variety of ways (see Sec. IV).

Figures 2 and 3 are diagrams of the over-all arrangements. A weak extracted beam of electrons produces tagged γ rays. These then interact in the hydrogen target, which is surrounded by hadron detectors.

The electron beam was derived from a weak circulating current in the synchrotron, which helped to reduce any background effects. The beam transport system has been described elsewhere.¹² The electron beam had a nominal spot size of 3 mm square and divergence of ± 0.37 mrad horizontally by ± 0.22 mrad vertically, at the converter R placed at the entrance to the tagging system. The beam spill from the machine could be made 1 to 2 msec long, at a repetition rate of 53 per second, and the spill could be made uniform by a servomechanism.¹³ The electron energy at the time of any event could be determined from machine clock pulses. The copper converter R was $1/200$ radiation length thick and $10 \text{ mm} \times 10 \text{ mm}$, and could be inserted or withdrawn by remote control.

A γ ray produced at the converter proceeded forwards, and the associated electron was deflected in vacuum by a focusing magnet M , essentially of sector type with parallel pole pieces 40 mm apart. The deflected electron could be detected in one of 64 accurately positioned counters E , providing its energy lay, nominally, between 237.5 MeV and 1837.5 MeV. It was then also detected in one of 16 backing counters B . A coincidence was demanded between an electron counter E , in a group of four, with the appropriate backing counter B . The 64 counters E thus covered together a nominal span of 1600 MeV, each counter corresponding to a non-

overlapping ± 12.5 -MeV width. Due to beam divergence and position effects the actual width is generally near to an overlapping ± 17.5 MeV. Some features of the tagging system have been detailed elsewhere.¹⁴ When working at beam energies greater than 3 GeV, the main electron beam was absorbed in an adjustable lead-lined front beam stop *A*. Otherwise this front beam stop was lowered, and the beam passed through a helium bag to a rear beam stop.

The tagged γ rays, after leaving the vacuum vessel of the tagging system, passed through a 100-mm diam hole in the lead-lined shielding wall *W*, and then through the 25-mm diam hole in a collimating veto counter *V*₁, on their way to the hydrogen target. This collimator counter had an outside diameter of 125 mm, and consisted of 16 lead-scintillator sandwiches, accurately aligned, each lead sheet being about 1 radiation length thick. A thick lead shield with a somewhat larger aperture lay to the rear. By this counter collimator device, beam halo effects could be successfully eliminated.

The liquid-hydrogen target cell was 200 mm long and 44 mm in diameter. The cylindrical walls of this were of stainless steel 0.25 mm thick, and the end windows were of moulded Mylar 0.12 mm thick. The superinsulated cell was enclosed in a vacuum jacket, the cylindrical walls of which were of stainless steel 0.5 mm thick, with steel flanges supporting Mylar windows 0.12 mm thick. A Philips cryogenerator and a helium-gas heat exchanger were used to liquefy a closed volume of hydrogen gas. The temperature of the target system was monitored with a vapor-pressure thermometer.

The main detector system of hadronic events consisted of six pairs of plastic scintillators of type NE 102A each 6 mm thick, forming the sides and ends of a rectangular box surrounding the target, except for beam entry and exit holes ~ 50 mm in diameter, and a small front slot for the target entry tube. The angle subtended at the center of the target by the exit hole in the downstream pair of detectors was $\pm 2.5^\circ$. The scintillators were coupled to photomultipliers of type RCA 8575.

A lead sheet 6 mm thick with a 50-mm diam hole in it was placed in front of the downstream pair of counters to assist in the detection of neutral pions. The main π^0 detector in the forward direction was a shower counter 600 mm square with a 150-mm diam central hole, downstream of *V*₂. This was made up of three separate counters, each with three radiation lengths of lead in front. Two of these counters were generally used, in coincidence. The box of inner scintillators was enclosed in 6 mm of lead and pairs of scintillators were placed around this to detect π^0 particles.

The shower counter *V*₂, for the vetoing of elec-

tromagnetic events and the detection of γ rays, consisted of a lead-scintillator sandwich 125 mm in diameter using 16 radiation lengths of lead interspersed with sheets of scintillator 6 mm thick. It could be placed in a variable position downstream. In practice one of two positions was employed; in one *V*₂ subtended an angle of $\pm 2.7^\circ$ for electromagnetic events at the target center, in the other $\pm 3.5^\circ$ at the target center. At the highest beam energies employed it would have been desirable to have made some measurements with the counter *V*₂ further back, but the space available in this part of the experimental area did not permit this. There were, in addition, electron veto counters *C*, consisting of a pair of scintillation counters in coincidence. Each counter carried a thin scintillator just under 70 mm square, 0.9 mm thick, the rear counter being 820 mm from the target center. A further veto counter *V*₀ was used to eliminate effects due to pair production in the radiator.

Auxiliary annular counters *F*, of various sizes, could be inserted in turn at the rear of the system. They were used to estimate the small loss of hadronic events in the forward cone occupied by the veto counters *V*₂ and *C*, by extrapolating the observations to zero angle.

B. Electronic Logic

A circuit diagram of the system is shown in Fig. 4. On the tagging-counter side a strobe coincidence was demanded between an electron counter and backing counter. On the hadron-counter side a coincidence between a pair of counters was subjected to possible vetos. A coincidence between a tagging pulse and a permitted hadronic pulse constituted an event, and activated the appropriate one of 64 one-bit stores. The event also started a 2-MHz clock which scanned the content of the stores, with the aid of coincidence units. Thus the number of clock pulses counted gave the tagging channel associated with the event, and this number was recorded on magnetic tape. If two tagging channels had fired, as happened only occasionally, both were recorded.

The tagged counts in each set of four electron counters in coincidence with the appropriate backing counter, which coincided with a shower-counter pulse, were also registered in 16 blind scalers, which could be read out at the end of a run. The over-all number of tagged γ rays was similarly recorded.

The number and distribution of random coincidences was determined as follows. Pulses from the hadron counters, which had not been suppressed by a veto signal, were delayed and subjected to a further veto, since there was a strong

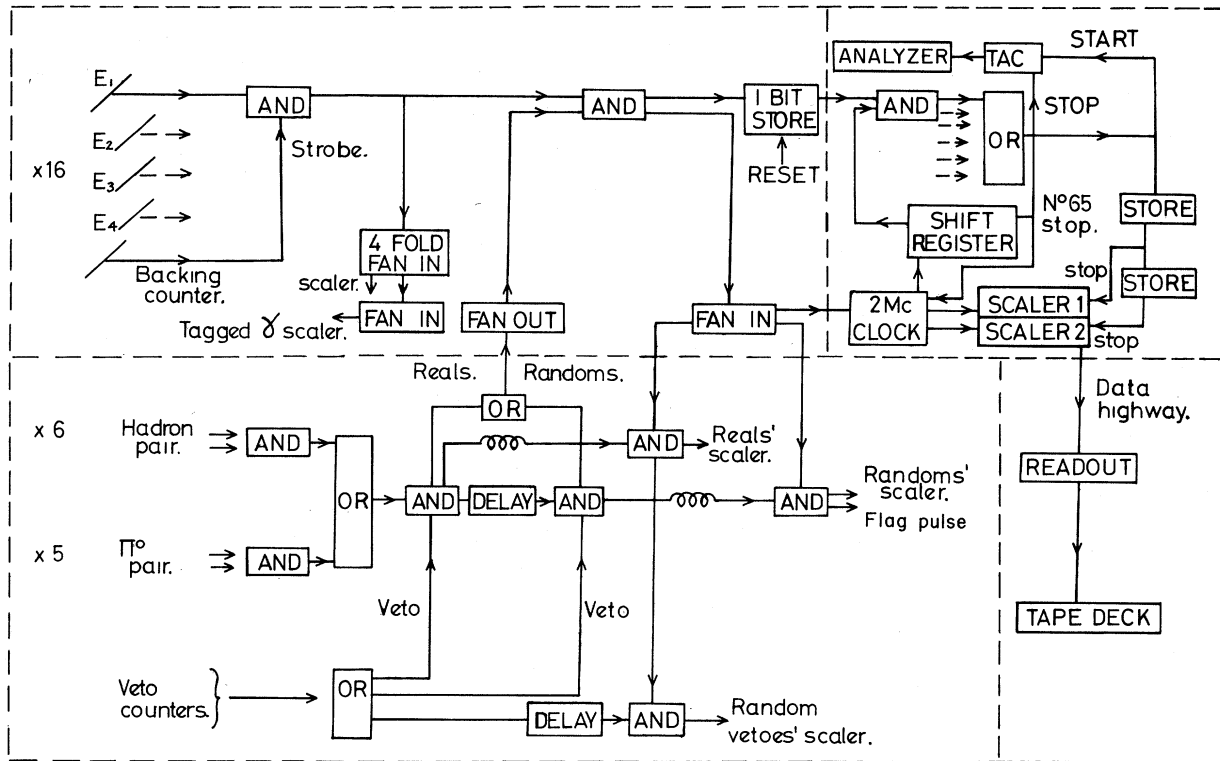


FIG. 4. Schematic diagram of electronics.

correlation between the veto counters and the tagging system. These pulses were put into coincidence with the tagging counters, along with real counts. The delay was made 735 nsec, the circulating time in the machine. After a coincidence occurred, a test was made to determine whether the event was an apparently real one or a delayed random one. A flag pulse, recorded on the tape, specified the nature of the event.

The number of events accidentally vetoed was estimated simultaneously, and the total number of these in any run was recorded.

In order to check on the number of events detected only in the π^0 arrays, the number of events in these counters not in coincidence with events in the hadron box could be determined.

By performing special runs, using only one of each set of four electron counters in turn in coincidence with the appropriate backing counter and the shower counter V_2 , the output of the tagging system could be compared, 16 channels at a time, with a bremsstrahlung spectrum.

IV. PROCEDURE AND RESULTS

Incident electron beam energies of 2.1, 2.4, 3.35, 3.5, and 4.6 GeV were used at various stages of the experiment. These gave tagged γ rays over

a nominal span of 0.275–4.35 GeV.

The response of the tagging system was regularly compared with that expected from bremsstrahlung at the various energies. Statistical accuracies of order $\frac{1}{4}\%$ per channel were realizable. The agreement was generally within a mean-square deviation of $\pm 1\frac{1}{2}\%$. It was therefore convenient to take the theoretical bremsstrahlung spectra as a basis for the total cross-section calculations. Whenever experimentally observed values were used as a check, little difference was observed in the form of the results. The tagging rate with radiator out was frequently compared with that with radiator in. The ratio was generally less than $\frac{1}{2}\%$.

Tagged γ -ray rates of up to 2×10^4 γ /sec were employed in total cross-section determinations and slow runs were interspersed with fast runs, to check on rate-dependent effects. Empty target runs were also carried out, the background amounting to about 20% of the full target rate. This background could be attributed in the main to the four windows of the target system, to the light-tight windows of the veto counter V_1 , and to air in the beam line following V_1 .

In the σ_T runs at 2.1 and 2.4 GeV, 300 000 events were accumulated. The 3.35- and 3.5-GeV runs contributed about 90 000 events and the 4.6-GeV runs about 100 000 events. The data obtained with

the various incident beam energies showed consistency over the regions of overlap. Large overlap in particular occurred for the 2.1-GeV and 2.4-GeV runs, and the structures revealed were in quantitative agreement over the common region. Just under half the data at the higher energies were taken with the veto counter V_2 in the rear position, subtending $\pm 2.7^\circ$. For the 2.1- and 2.4-GeV runs this veto counter subtended $\pm 3.5^\circ$. Running conditions, such as discriminator settings, were adjusted to maintain the efficiency of the vetoing system for the different beam energies.

Since the efficiency of the shower counter V_2 is extremely important, its properties have been studied in detail. Its resolution has been measured, and found to be adequate. For example it was 18% full width at half-maximum (FWHM) for 3.5-GeV electrons. Its measured detection efficiency for 3.5-GeV electrons was greater than 99.8%. The difference between this and our calculated value of 99.96% can be explained by a small amount of low-energy contamination of the electron beam. Each electron counter was found to be at least 98% efficient. Hence the minimum efficiency of the vetoing system was 99.8% for photons, and 99.99% for electrons or positrons, of this energy. These assessments confirmed that electromagnetic events were adequately suppressed, and that no corrections were necessary for them.

The π^0 counters were found to give little contribution, except near the first resonance. At the first resonance a backward-going proton from the reaction $\gamma + p \rightarrow p + \pi^0$ would not escape from the target with sufficient energy to be detected, but a forward-going neutral pion would be counted.

By using the electron counters with the hadron ones as detectors, and removing V_2 and the electron counters from the veto system, the electro-

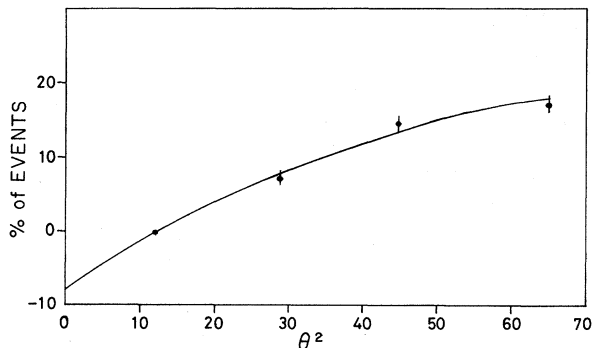


FIG. 5. Forward-angle correction curve for hydrogen, showing the percentage of hadronic events emitted within an angle θ of a tagged γ beam derived from a 4.6-GeV electron beam. The true zero of the vertical scale is where the curve meets the vertical axis. For $\theta = 2.7^\circ$, the correction is 5%.

magnetic cross section of hydrogen was determined. These and related measurements will be reported later.

Data were collected from the annular counters to estimate the loss of hadronic events in the forward cone covered by the veto shower and electron counters. Figure 5 summarizes some of the results obtained with an incident electron beam energy of 4.6 GeV. It shows the percentage of hadronic events with a product particle inside an angle θ , as a function of θ^2 , representing the solid angle. The true zero of the vertical scale is where the curve meets the vertical axis. The average corrections for losses are shown in Table I, for varying beam energy and shower-counter position. These figures take into account the fact that the counter is only partially efficient for hadron detection, since charged pions must convert to neutral pions before a shower can build up. Further measurements were made with deuterium and other elements, which agreed with these results. We have also estimated this forward correction by analyzing a data tape from the Aachen-Berlin-Bonn-Hamburg-Heidelberg-München Collaboration (ABBHMM) bubble-chamber experiment.¹¹ Plots of particle yields as a function of angle were carried out for several energy bands. The results were in close accord with those derived using the annular counters. The corrections for losses in the forward direction, which had to be applied to the hydrogen data as a whole rose steadily, therefore, in known fashion from approximately 0 at a nominal 275 MeV to +8% at a nominal 4.225 GeV, the highest γ -ray energy point considered here. At the other end, over-all hadron losses amounted to +2% at the lowest energy.

Other corrections were much smaller. Double bremsstrahlung losses, effective-length effects, and bubbling losses in the hydrogen target were considered small, of order 1% in all. Counting losses and absorption in the target amount to about 1%.

The presence of counts in more than one channel caused, generally, an uncertainty of $\pm 1\%$ in the

TABLE I. Forward-angle corrections.

Shower-counter angle (degrees)	Incident energy (GeV)	Percentage of events vetoed
2.7	3.5	3.0 ± 1.0
	4.6	5.0 ± 1.5
3.5	3.5	4.0 ± 1.5
	4.6	7.0 ± 2.0

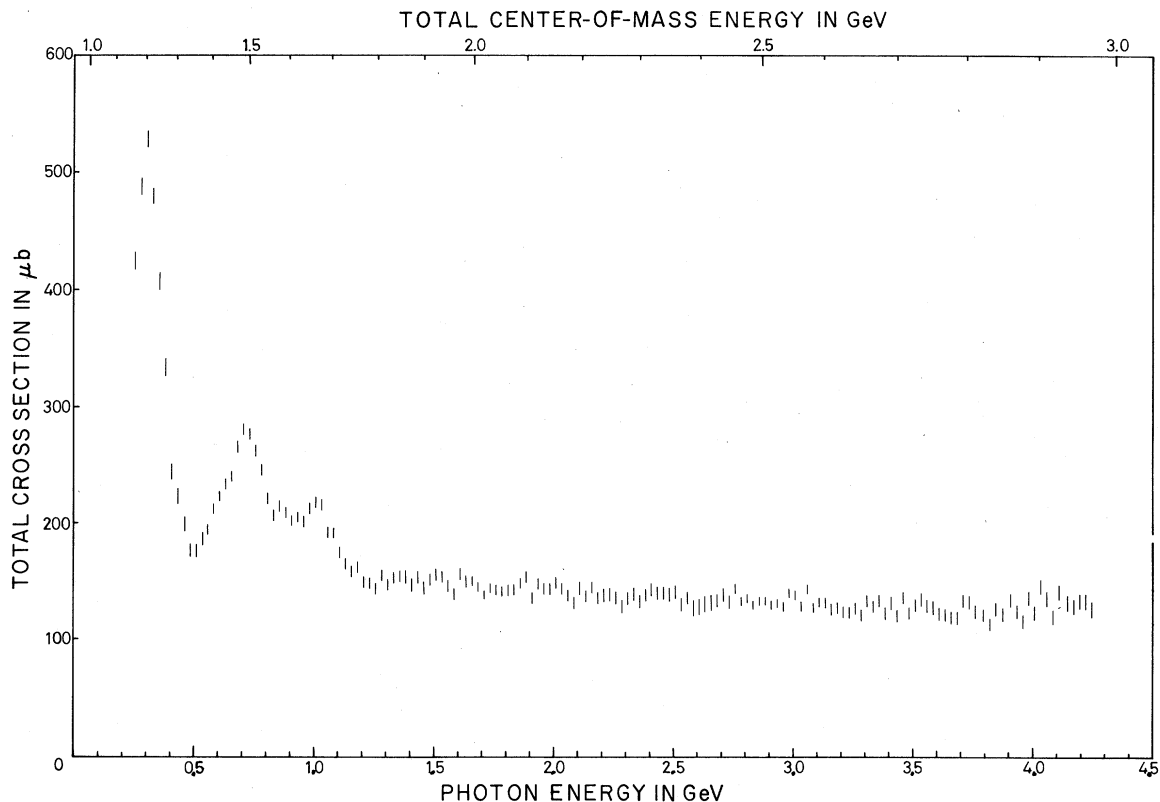


FIG. 6. The total photon-proton hadronic cross section as a function of γ -ray energy. The numerical values are listed in Table II.

cross section. Random counts and background contributions tended to be concentrated in the first channels of the tagging system (i.e., that corresponding to electrons centered at 250 MeV, and the channels immediately following it). Any low-energy electron contamination in the beam would tend to go preferentially there. In the final plot only data from the last 59 channels were therefore employed.

Figure 6 shows data on σ_T for hydrogen over the energy range investigated. A small correction (10 MeV) has been made which takes account of the energy variation in the recorded beam spill below 2 GeV. A recent calibration of the synchrotron magnets indicates that the incident electron energies of 2.1 GeV and 2.4 GeV lie very near the true values. The position of the 1st resonance peak therefore lies close to a γ energy of 0.315 GeV.

Table II lists the values of σ_T at the various γ -ray energies. The errors ($\pm\Delta\sigma_T$) given are the statistical ones. To these should be added the bremsstrahlung deviations amounting to $\pm 1\frac{1}{2}\%$ below 2 GeV. At other energies they play no important role. Finally the systematic errors (which vary slowly with energy), in specifying the absolute cross sections can amount to an additional $\pm 3\%$.

In order to determine the extent of inherent channel-to-channel variations in a diagram like Fig. 6, another, subsidiary, experiment was carried out. This was designed as an over-all check on the response of the hadron counters and their timing relative to the individual tagging channels. A sheet of lead 3 mm thick was placed in the beam just outside the wall W to produce electromagnetic events which would scatter into the detectors. All veto counters were switched off, and if all the channels were operating correctly, a smooth curve of channel counts versus channel number could be expected. If this were divided by the bremsstrahlung spectral distribution, a steady curve free from variations should result. Figure 7 shows such a set of results obtained for 150 000 events with incident electron energies 3.35 and 4.6 GeV. Analysis shows there are no marked variations outside the statistical inaccuracies.

V. ANALYSIS AND DISCUSSION

A. General Characteristics

The results (Fig. 6) permit the form of the curve in the region below 1.8 GeV to be expressed fairly definitely. The P_{33} (1236 MeV) state and the features

TABLE II. Total cross-section results.

ν (GeV)	σ_T (μb)	$\Delta\sigma_T$ (μb)	ν (GeV)	σ_T (μb)	$\Delta\sigma_T$ (μb)	ν (GeV)	σ_T (μb)	$\Delta\sigma_T$ (μb)
0.265	424.5	8.0	1.590	138.8	5.1	2.915	130.4	3.9
0.290	487.0	8.1	1.615	156.5	5.1	2.940	131.4	4.0
0.315	526.9	8.1	1.640	150.2	5.0	2.965	128.7	4.0
0.340	477.8	8.3	1.665	150.3	4.0	2.990	140.4	4.0
0.365	406.6	8.0	1.690	145.4	3.9	3.015	138.3	4.1
0.390	334.1	7.6	1.715	138.9	3.7	3.040	129.2	4.3
0.415	244.4	7.5	1.740	144.5	3.9	3.065	143.6	4.0
0.440	224.5	6.7	1.765	142.5	4.4	3.090	128.0	4.2
0.465	200.5	6.6	1.790	141.5	4.5	3.115	132.6	4.0
0.490	178.3	6.5	1.815	142.4	4.7	3.140	132.1	4.4
0.515	176.9	6.4	1.840	143.2	4.4	3.165	126.8	5.0
0.540	186.9	6.2	1.865	148.6	4.4	3.190	127.8	5.1
0.565	194.0	4.0	1.890	153.9	4.7	3.215	124.3	4.9
0.590	211.7	3.9	1.915	135.4	4.6	3.240	123.9	4.9
0.615	222.6	4.1	1.940	148.0	4.9	3.265	127.1	5.2
0.640	232.7	4.2	1.965	144.3	4.7	3.290	121.3	5.0
0.665	239.5	4.3	1.990	143.5	4.7	3.315	133.8	5.1
0.690	264.6	4.5	2.015	149.1	4.8	3.340	128.7	5.1
0.715	279.0	4.5	2.040	143.5	5.2	3.365	134.3	5.2
0.740	275.6	4.6	2.065	138.0	5.3	3.390	123.1	5.1
0.765	260.7	4.6	2.090	131.7	5.3	3.415	131.7	5.4
0.790	244.7	4.6	2.115	144.5	5.2	3.440	121.4	5.3
0.815	221.1	4.6	2.140	137.5	5.3	3.465	137.0	5.2
0.840	206.3	4.6	2.165	144.9	5.3	3.490	123.2	5.2
0.865	213.7	4.5	2.190	135.9	5.3	3.515	130.1	5.4
0.890	208.8	4.5	2.215	138.3	5.4	3.540	134.8	5.4
0.915	201.7	4.7	2.240	139.0	5.5	3.565	129.4	5.3
0.940	205.0	4.6	2.265	136.1	5.5	3.590	127.8	6.0
0.965	201.5	4.8	2.290	128.6	5.5	3.615	122.7	5.7
0.990	212.1	4.9	2.315	135.9	5.6	3.640	121.8	5.5
1.015	217.5	5.0	2.340	139.5	5.8	3.665	119.8	5.6
1.040	215.2	4.9	2.365	132.7	5.5	3.690	119.3	5.7
1.065	191.7	5.0	2.390	138.7	5.6	3.715	134.2	5.4
1.090	191.1	5.0	2.415	143.1	5.7	3.740	132.3	5.5
1.115	174.7	5.0	2.440	140.3	5.8	3.765	124.8	5.8
1.140	165.0	4.8	2.465	140.4	5.6	3.790	122.0	5.6
1.165	158.7	4.9	2.490	138.9	6.1	3.815	113.9	5.5
1.190	162.2	5.0	2.515	141.0	5.8	3.840	127.1	6.0
1.215	149.6	4.8	2.540	130.4	5.8	3.865	122.4	5.9
1.240	148.6	5.0	2.565	136.3	5.7	3.890	134.7	5.9
1.265	143.8	4.9	2.590	124.1	7.7	3.915	124.9	5.7
1.290	155.6	4.7	2.615	128.4	7.0	3.940	116.3	5.8
1.315	146.8	4.9	2.640	129.9	7.7	3.965	136.2	6.1
1.340	153.6	4.8	2.665	132.5	7.3	3.990	123.6	6.3
1.365	154.4	5.0	2.690	134.3	5.9	4.015	146.2	6.3
1.390	153.6	5.4	2.715	138.7	6.0	4.040	135.6	6.3
1.415	146.8	5.2	2.740	132.8	6.1	4.065	119.8	6.6
1.440	153.5	5.3	2.765	144.4	4.3	4.090	141.9	6.8
1.465	144.2	5.4	2.790	133.4	4.1	4.115	132.4	6.9
1.490	151.5	5.2	2.815	136.2	3.8	4.140	128.8	6.5
1.515	155.9	5.3	2.840	130.2	4.0	4.165	133.6	6.8
1.540	154.1	5.1	2.865	133.8	3.7	4.190	133.5	7.2
1.565	146.1	5.1	2.890	133.9	3.8	4.215	126.6	6.9

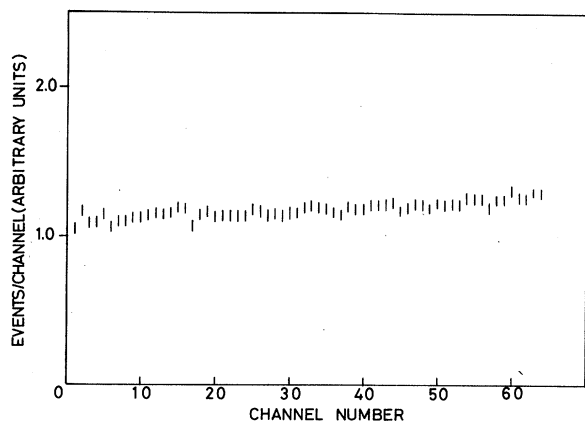


FIG. 7. Over-all uniformity check on the system (see text).

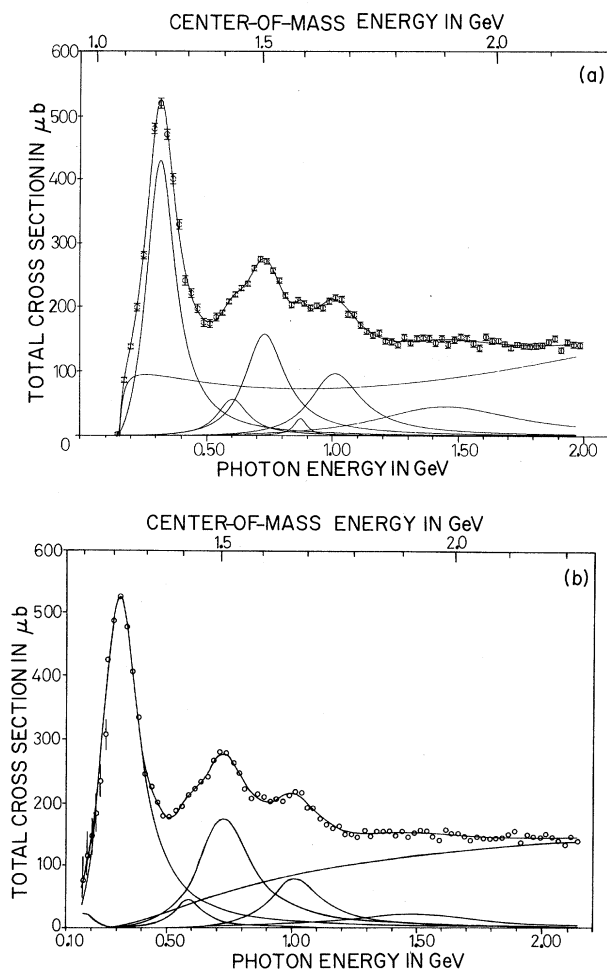


FIG. 8. (a) Fit to data using a background $\sum_{n=-2}^{+2} C_n (W - W_0)^n$, where W and W_0 are center-of-mass energies at ν and ν_0 . The four points above threshold come from Ref. 18. (b) Fit to data using a background $\sum_{n=1}^5 C_n (\nu - \nu_0) \nu^{-n}$. The six points above threshold come from Ref. 2.

of the 2nd and 3rd resonances, often loosely associated with the D_{13} (1520 MeV) and F_{15} (1688 MeV) states, respectively, are clearly seen. There is evidence of a small broad enhancement in the mass region of 1900 MeV. There is also a shoulder at a position sometimes allocated to a P_{11} state of mass near 1470 MeV, but which can also be assigned to a threshold effect. For γ -ray energies above 1850 MeV the deviations from a smooth curve are not significantly greater than the statistical variations. Possible enhancements in this region must therefore necessarily be very small, if present. The over-all trend in the 1.85–4.225-GeV region is essentially that of a steadily falling cross section. These and related matters are considered further below.

B. The Spin-Averaged Forward Scattering Amplitude f_1

In order to evaluate the principal-value integral in the dispersion relation of Sec. II it is necessary to have a smooth fit to the data. Two fits have been used in the resonance region.

In the two fits, five and six resonance forms were used corresponding to the main features of the region. These were given the Breit-Wigner parametrization of Walker.¹⁵ Another difference between the fits was in the shape given to the background. In fit I this was of the form $\sum_{n=-2}^{+2} C_n (W - W_0)^n$, where W is the center-of-mass energy and W_0 is the value corresponding to the pion photoproduction threshold. The minimization was performed using the program VA04A.¹⁶ Fit II used a background of the form $\sum_{n=1}^5 C_n (\nu - \nu_0) \nu^{-n}$ and the minimization was performed by the CERN program MINUIT.¹⁷ Fits I and II, and the individual contributions from each resonance, and from the background, are shown in Figs. 8(a) and 8(b),¹⁸ respectively. The background contribution at low energies in fit I is representative of the S wave and other Born terms.

The two over-all fits produced very similar values of χ^2 , and are therefore very alike. Due to the very different background forms used, however, the resonance parameters are rather different in the two cases. One common feature however is the low mass and narrow width found for the possible P_{11} state (mass 1400–1430 MeV). Fit I has a small peak at a mass value of 1590 MeV.

The high-energy data were initially fitted to the Regge form $(a_1 + a_2 \nu^{-1/2})$ as explained in Sec. II. The value found was

$$\sigma_T = 91.0 + 71.4 \nu^{-1/2} \mu\text{b}.$$

More explicitly $a_1 = 91.0 \pm 5.6$, $a_2 = 71.4 \pm 9.6$. The errors quoted were extracted from the variance matrix. The fit is shown in Fig. 9. The fits in the resonance region and at high energy merge

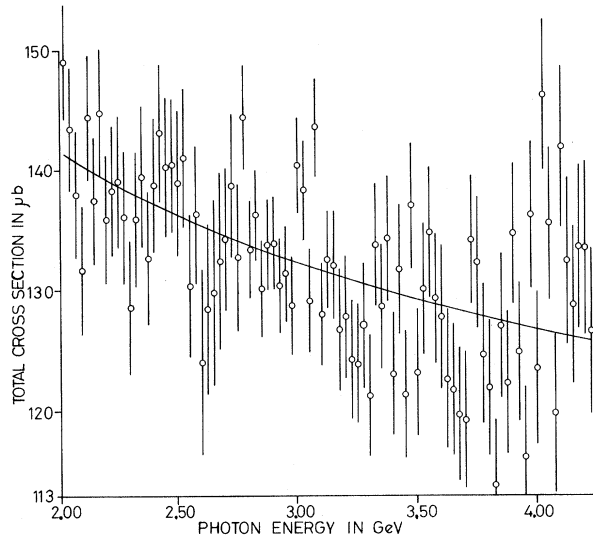


FIG. 9. High-energy fit.

satisfactorily at their junctions, so as to give an over-all fit for the complete energy band from threshold to 4.215 GeV. The high-energy data are not extensive enough to allow a simultaneous fit to $\alpha(0)$ in the more general expression

$$\sigma_T(\nu) = a'_1 + a'_2 \nu^{\alpha(0)-1}.$$

However, since any value of $\alpha(0)$ between 0.4 and 0.6 would seem reasonable,⁷ alternative fits have been performed for these two extreme cases. The results together with those for the $\alpha(0)=0.5$ case are presented in Table III.

For comparison, in the case $\alpha(0)=0.5$, Meyer *et al.*³ found a value for σ_T of $(95 + 64 \nu^{-1/2}) \mu\text{b}$, and Caldwell *et al.*⁴ a value of $(94.1 + 79.0 \nu^{-1/2}) \mu\text{b}$.

$\text{Im} f_1(\nu)$ was calculated via the optical theorem from the smooth fit to the data and used in the dispersion relation Eq. (2a) to calculate $\text{Re} f_1(\nu)$. The integration was carried out using the CERN principal-value-integration routine CAUCHY. Values of $\text{Im} f_1$ and $\text{Re} f_1$ for the photon laboratory energies employed in the experiment are given in Table IV, for the fit combining fit II and the high-energy fit. The values of $\text{Im} f_1$ and $\text{Re} f_1$ for the two over-all fits generally differ little from one another.

TABLE III. Regge parameters.

$\alpha(0)$	a_1	a_2	C
0.4	97.9	66.2	-0.8
0.5	91.0	71.4	-2.3
0.6	80.7	80.0	-3.3

The Argand diagram, Fig. 10, shows the loops due to the P_{33} , D_{13} , and F_{15} resonances. The two inflections near 600-MeV and 1500-MeV γ energy are due to the shoulder on the second resonance—possibly due to the P_{11} , and the fourth resonance F_{37} , respectively.

The σ_T data in the resonance region generally accord with the extrapolated values derived from the SLAC electron scattering experiments, bearing in mind quoted error limits.

The finite-energy sum rule Eq. (5c) has been used to evaluate the fixed-pole contribution C . Using $\alpha=0.5$, $a_1=91.0$, $a_2=71.4$, $N=4.0$ GeV, C is determined at $-2.3 \mu\text{b}$ GeV, a value in the neighborhood of the Thomson limit of $-3 \mu\text{b}$ GeV. However one should be somewhat guarded about the precise value of C . Though it is not appreciably influenced by the value of N , it is dependent on the choice of the exponent α (see Table III).

C. Compton Scattering

Experiments from CEA, DESY, and SLAC on Compton scattering were recently reported at the Cornell conference. Writing Eq. (3) as

$$\left. \frac{d\sigma(\gamma p \rightarrow \gamma p)}{dt} \right|_{t=0} = \frac{\sigma_T^2}{16\pi} \left[1 + \left(\frac{\text{Re} f_1(\nu)}{\text{Im} f_1(\nu)} \right)^2 \right] + \frac{\pi}{\nu^2} |f_2(\nu)|^2, \quad (7)$$

comparisons of Compton scattering data¹⁹ with the present σ_T values confirm the small contribution of f_2 over the γ range 2–4 GeV. Quantitatively $|f_2|^2 < 0.1 |f_1|^2$.

D. Vector-Dominance Model

At 4 GeV the quark model predicts

$$\begin{aligned} \sigma_T(\rho_0 p) &= \sigma_T(\omega p) \\ &= \frac{1}{2} [\sigma_T(\pi^+ p) + \sigma_T(\pi^- p)] = 30 \text{ mb} \end{aligned}$$

and

$$\sigma_T(\phi p) = 15 \text{ mb}.$$

Using a σ_T value given by the relation (91 + 71.4 $\nu^{-1/2}$) mentioned earlier, i.e., 127 μb at 4 GeV, and assuming

$$1/\gamma_\rho^2 : 1/\gamma_\omega^2 : 1/\gamma_\phi^2 = 9 : 1 : 2$$

according to SU(6), Eq. (6) gives $\gamma_\rho^2/4\pi = 0.53$. The contribution to the error on this from uncertainties in cross-section values amounts to about $\pm 5\%$. This compares with a value of 0.64 ± 0.05 from the Orsay storage rings.²⁰

TABLE IV. Spin-averaged forward scattering amplitude, f_1 .

ν (GeV)	$Re f_1$	$Im f_1$	ν (GeV)	$Re f_1$	$Im f_1$	ν (GeV)	$Re f_1$	$Im f_1$
0.000	-3.0	0.0	1.365	-9.6	16.2	2.815	-11.7	29.9
0.020	-3.0	0.0	1.390	-9.5	16.5	2.840	-11.8	30.1
0.040	-2.9	0.0	1.415	-9.5	16.9	2.865	-11.8	30.3
0.060	-2.7	0.0	1.440	-9.5	17.3	2.890	-11.9	30.6
0.080	-2.5	0.0	1.465	-9.6	17.6	2.915	-11.9	30.8
0.100	-2.2	0.0	1.490	-9.7	17.9	2.940	-11.9	31.0
0.120	-1.7	0.0	1.515	-9.8	18.2	2.965	-12.0	31.2
0.140	-1.0	0.0	1.540	-9.9	18.5	2.990	-12.0	31.5
0.160	0.1	0.4	1.565	-10.0	18.7	3.015	-12.0	31.7
0.180	0.9	1.1	1.590	-10.1	18.9	3.040	-12.1	31.9
0.200	1.9	2.1	1.615	-10.2	19.0	3.065	-12.1	32.1
0.220	2.8	3.5	1.640	-10.3	19.2	3.090	-12.1	32.4
0.240	3.5	5.4	1.665	-10.3	19.4	3.115	-12.2	32.6
0.260	3.5	7.9	1.690	-10.3	19.5	3.140	-12.2	32.8
0.265	3.3	8.5	1.715	-10.3	19.7	3.165	-12.3	33.0
0.290	1.5	11.5	1.740	-10.3	19.9	3.190	-12.3	33.3
0.315	-1.5	13.2	1.765	-10.3	20.1	3.215	-12.3	33.5
0.340	-4.6	13.0	1.790	-10.3	20.3	3.240	-12.4	33.7
0.365	-6.6	11.7	1.815	-10.3	20.5	3.265	-12.4	33.9
0.390	-7.5	10.1	1.840	-10.2	20.8	3.290	-12.4	34.1
0.415	-7.6	8.8	1.865	-10.2	21.0	3.315	-12.5	34.4
0.440	-7.2	7.8	1.890	-10.2	21.3	3.340	-12.5	34.6
0.465	-6.5	7.2	1.915	-10.2	21.6	3.365	-12.5	34.8
0.490	-5.6	7.0	1.940	-10.3	21.8	3.390	-12.6	35.0
0.515	-4.6	7.1	1.965	-10.3	22.1	3.415	-12.6	35.2
0.540	-3.7	7.7	1.990	-10.3	22.4	3.440	-12.6	35.5
0.565	-3.0	8.8	2.015	-10.5	22.7	3.465	-12.7	35.7
0.590	-3.0	9.9	2.040	-10.5	22.9	3.490	-12.7	35.9
0.615	-2.9	10.7	2.065	-10.6	23.1	3.515	-12.8	36.1
0.640	-2.8	11.7	2.090	-10.7	23.4	3.540	-12.8	36.3
0.665	-2.8	13.1	2.115	-10.7	23.6	3.565	-12.8	36.6
0.690	-3.5	14.5	2.140	-10.7	23.8	3.590	-12.9	36.8
0.715	-4.8	15.6	2.165	-10.8	24.0	3.615	-12.9	37.0
0.740	-6.3	16.1	2.190	-10.8	24.2	3.640	-12.9	37.2
0.765	-7.6	15.8	2.215	-10.8	24.4	3.665	-13.0	37.4
0.790	-8.4	15.3	2.240	-10.9	24.7	3.690	-13.0	37.7
0.815	-8.8	14.7	2.265	-10.9	24.9	3.715	-13.0	37.9
0.840	-8.8	14.2	2.290	-10.9	25.1	3.740	-13.1	38.1
0.865	-8.5	14.0	2.315	-11.0	25.4	3.765	-13.1	38.3
0.890	-8.1	14.1	2.340	-11.0	25.6	3.790	-13.1	38.5
0.915	-7.8	14.6	2.365	-11.1	25.8	3.815	-13.2	38.8
0.940	-7.7	15.3	2.390	-11.1	26.0	3.840	-13.2	39.0
0.965	-8.0	16.1	2.415	-11.1	26.3	3.865	-13.2	39.2
0.990	-8.7	16.8	2.440	-11.2	26.5	3.890	-13.3	39.4
1.015	-9.7	17.2	2.465	-11.2	26.7	3.915	-13.3	39.6
1.040	-10.6	17.1	2.490	-11.2	27.0	3.940	-13.3	39.9
1.065	-11.3	16.6	2.515	-11.3	27.2	3.965	-13.4	40.1
1.090	-11.6	16.1	2.540	-11.3	27.4	3.990	-13.4	40.3
1.115	-11.7	15.6	2.565	-11.4	27.6	4.015	-13.4	40.5
1.140	-11.5	15.2	2.590	-11.4	27.9	4.040	-13.5	40.7
1.165	-11.4	15.0	2.615	-11.5	28.1	4.065	-13.5	40.8
1.190	-11.1	14.8	2.640	-11.5	28.3	4.090	-13.5	41.2
1.215	-10.8	14.8	2.665	-11.5	28.5	4.115	-13.6	41.4
1.240	-10.6	14.9	2.690	-11.6	28.8	4.140	-13.6	41.6
1.265	-10.3	15.0	2.715	-11.6	29.0	4.165	-13.6	41.8
1.290	-10.1	15.3	2.740	-11.6	29.2	4.190	-13.7	42.0
1.315	-9.9	15.5	2.765	-11.7	29.4	4.215	-13.7	42.3
1.340	-9.7	15.8	2.790	-11.7	29.7	4.240	-13.7	42.5

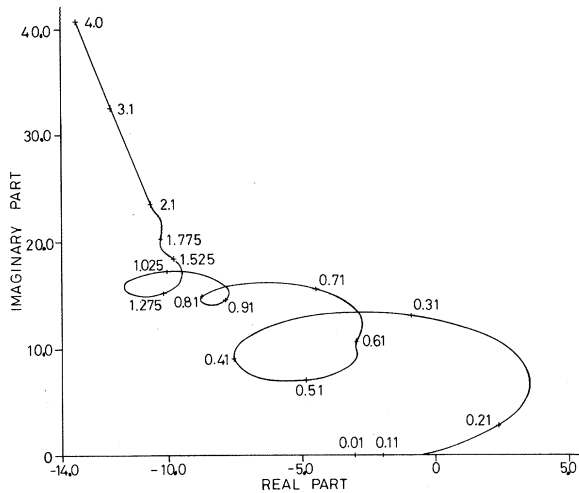


FIG. 10. Argand diagram for the forward scattering amplitude $f_1(\nu)$, plotted as ν goes from 0 to 4.0 GeV.

E. Concluding Remarks

It is of interest to compare the values of $\sigma_T(\gamma p)$ with a compilation of cross sections of measured photoproduction processes. From threshold to a γ energy of 2 GeV, σ_T is dominated by singly- and triply-charged final states. The measured total cross sections for the following reactions have been summed for this energy range^{11, 18, 21-23}

$$\begin{aligned} &\gamma p \rightarrow p\pi^0, \quad \gamma p \rightarrow n\pi^+, \quad \gamma p \rightarrow p\pi^+\pi^-, \quad \gamma p \rightarrow p\eta, \\ &\gamma p \rightarrow p\pi^+\pi^-\pi^0 \text{ (plus neutrals)}, \\ &\gamma p \rightarrow n\pi^+\pi^-\pi^+ \text{ (plus neutrals)}, \\ &\gamma p \rightarrow \text{strange particles}. \end{aligned}$$

The result is shown in Fig. 11, together with data from this experiment. The uncertainties in the compilation, originating from the stated errors in the above individual determinations vary from $\sim 3\%$ at 300 MeV to $\sim 5\%$ at 1 GeV. There is no real discrepancy in the region of the first resonance. There is distinct evidence of structure in the difference between the compilation and our experimental values above this. At a γ -ray energy of 750 MeV the difference rises to $60 \pm 10 \mu\text{b}$; and at a γ -ray energy of 1050 MeV the difference peaks at $40 \pm 10 \mu\text{b}$. This is to be compared with an essentially constant discrepancy above 1.4 GeV of about $25 \mu\text{b}$. The difference data allow an assessment to be made of certain resonance processes.

Bubble-chamber data in the neighborhood of the second resonance have shown that the reaction $\gamma p \rightarrow p\pi^+\pi^-$ is dominated by the production of a $\Delta^{++}(1236)\pi^-$ combination to the extent of a contribution of $65 \mu\text{b}$ towards the total cross section of $71 \mu\text{b}$. If the effective 1520-MeV state is assumed

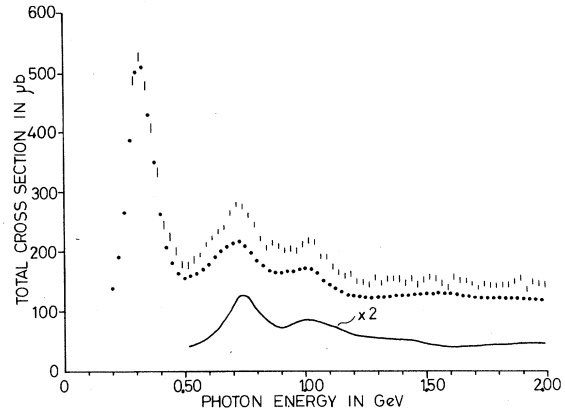


FIG. 11. Compilation of measured cross sections of component processes in aggregate shown as dots (●), with σ_T data plotted for comparison. The curve is a measure of the real difference, and is associated with the processes $\gamma p \rightarrow p\pi^0\pi^0$ and $\gamma p \rightarrow n\pi^+\pi^0$.

to be dominantly $l = \frac{1}{2}$, then the ratio of the $\Delta^{++}\pi^-$, $\Delta^+\pi^0$, $\Delta^0\pi^+$ states associated with its decay would be, using the appropriate Clebsch-Gordan coefficients, 3:2:1. $\Delta^+\pi^0$ would give rise to final states with two neutral particles ($p\pi^0\pi^0$ and $n\pi^+\pi^0$) and $\frac{2}{3}$ of the $\Delta^0\pi^+$ would lead to two neutrals ($n\pi^+\pi^0$). Thus $\frac{4}{9}$ of the decay of the $l = \frac{1}{2}$ state via $\Delta\pi$ gives rise to neutral states; the remaining $\frac{5}{9}$ leads to the $p\pi^+\pi^-$ final state ($\frac{9}{10}$ via $\Delta^{++}\pi^-$ and $\frac{1}{10}$ via $\Delta^0\pi^+$ - a total cross section therefore of $65 + 7 = 72 \mu\text{b}$), i.e., all the $p\pi^+\pi^-$ total cross section is $\Delta\pi$ production. If it is assumed that production of $\Delta\pi$ proceeds through the decay of the $l = \frac{1}{2}$, 1520 state and that any background is also $l = \frac{1}{2}$, then $\frac{4}{5}$ of $72 \mu\text{b}$, i.e., $58 \mu\text{b}$, would not be included in the compilation. The observed difference agrees satisfactorily with this scheme of things. On the other hand, the amount of $p\pi^-\pi^+$ from $\Delta^0\pi^+$ seen in bubble-chamber work was less than the $7 \mu\text{b}$ expected, so some interference between $\Delta^{++}\pi^-$ and $\Delta^0\pi^+$ amplitudes in yielding $p\pi^+\pi^-$ was postulated at that time.

Referring similarly to bubble-chamber work in the third resonance region, $50 \mu\text{b}$ of $\Delta^{++}(1236)\pi^-$ production was seen, as the mechanism of $p\pi^+\pi^-$ production. Taking the effective 1688-MeV state to be $l = \frac{1}{2}$, some $40 \mu\text{b}$ of states with two neutral and one charged particle would be expected outside the compilation. This too agrees with Fig. 11.

We have considered above some over-all consequences of the interaction of γ rays with protons at high energies. We hope to complete shortly an analysis of the deuteron total cross section. The above data will then be used to extract information on γ -neutron collisions.

ACKNOWLEDGMENTS

We thank our colleagues S. Hinds, A. D. Kanaris, P. G. Murphy, M. D. Rousseau, J. G. Rutherglen, and A. G. Wardle for their help in the initial stages of this project. We are grateful also to the ABBHHM group, especially P. Söding, for the loan of data tape, and to H. Meyer of DESY.

We are indebted to T. W. Aitken and other members of the Machine Division and greatly appreciate the assistance given by the Cryogenics, Engineering and Computer Groups at the Daresbury Laboratory. We are grateful to our universities for their support in this work.

Research grants from the Science Research Council were held by four of us (T.A.A., J.H.F., A.F.K., and A.W.R.) during these investigations.

*Present address: Department of Physics, University of Surrey, Guildford, Surrey, England.

¹J. Ballam, G. B. Chadwick, R. Gearhart, Z. G. T. Guiragossian, P. R. Klein, A. Levy, M. Menke, J. J. Murray, P. Seyboth, G. Wolf, C. K. Sinclair, H. H. Bingham, W. B. Fretter, K. C. Moffett, W. J. Podolsky, M. S. Rabin, A. H. Rosenfeld, and R. Windmolders, *Phys. Rev. Letters* **23**, 498 (1969). See also J. Ballam, G. B. Chadwick, Z. G. T. Guiragossian, P. R. Klein, A. Levy, M. Menke, E. Pickup, P. Seyboth, T. H. Tan, and G. Wolf, *ibid.* **21**, 1544 (1968).

²E. D. Bloom, R. L. Cottrell, D. H. Coward, H. de Staebler, Jr., J. Drees, G. Miller, L. W. Mo, R. E. Taylor, J. I. Friedman, G. C. Hartmann, and H. W. Kendall, SLAC Report No. SLAC-PUB-653, 1969 (unpublished).

³H. Meyer, B. Naroska, J. H. Weber, M. Wong, V. Heynen, E. Mandelkow, and D. Notz, *Phys. Letters* **33B**, 189 (1970).

⁴D. O. Caldwell, V. B. Elings, W. P. Hesse, R. J. Morrison, F. V. Murphy, B. W. Worster, and D. E. Yount, *Phys. Rev. Letters* **25**, 609 (1970).

⁵(a) T. A. Armstrong, W. R. Hogg, G. M. Lewis, A. W. Robertson, G. R. Brookes, A. S. Clough, J. H. Freeland, W. Galbraith, A. F. King, W. R. Rawlinson, N. R. S. Tait, J. C. Thompson, and D. W. L. Tolfree, *Phys. Letters* **34B**, 535 (1971). (b) See also in *Proceedings of International Symposium on Electron and Photon Interactions at High Energies, 1971*, edited by N. B. Mistry (Cornell Univ. Press, Ithaca, N.Y., 1972), Paper 195.

⁶M. Gell-Mann and M. L. Goldberger, *Phys. Rev.* **96**, 1433 (1954).

⁷M. Damashek and F. J. Gilman, *Phys. Rev. D* **1**, 1319 (1970).

⁸R. L. Anderson, D. Gustavson, J. Johnson, I. Overman, D. Ritson, B. H. Wiik, R. Talman, J. K. Walker, and D. Worcester, *Phys. Rev. Letters* **25**, 1218 (1970).

⁹C. A. Dominguez, C. Ferro Fontan, and R. Suaya, *Phys. Letters* **31B**, 365 (1970).

¹⁰H. Joos, DESY Report No. 67-13, 1967 (unpublished).

¹¹R. Erbe, H. G. Hilpert, E. Schuttler, W. Struczinski, K. Lanus, A. Meyer, A. Pose, H.-J. Schreiber, K. Böckmann, J. Moebos, H. Mück, B. Nellen, W. Tejjessy, G. Horlitz, E. Lohrmann, H. Meyer, W. P. Swan-

son, M. W. Teucher, G. Wolf, S. Wolff, D. Lüke, P. Söding, H. Spitzer, F. Storim, H. Beisel, H. Filthuth, P. Steffen, P. Freund, K. Gottstein, N. Schmitz, P. Seyboth, and J. Seyerlein, *Phys. Rev.* **175**, 1669 (1968). See also Aachen-Berlin-Bonn-Hamburg-Heidelberg-München Collaboration, *ibid.* **188**, 2060 (1969).

¹²T. W. Aitken, Daresbury Report No. DNPL/TM 63, 1970 (unpublished).

¹³T. W. Aitken and V. P. Suller, *Nucl. Instr. Methods* **83**, 176 (1970).

¹⁴G. R. Brookes, S. Hinds, W. R. Rawlinson, M. D. Rousseau, D. W. L. Tolfree, and A. G. Wardle, *Nucl. Instr. Methods* **85**, 125 (1970).

¹⁵R. L. Walker, *Phys. Rev.* **182**, 1729 (1969).

¹⁶M. J. D. Powell, *Computer J.* **7**, 155 (1964).

¹⁷F. James and M. Roos, CERN Computer Library Report No. D506, 1969 (unpublished).

¹⁸J. T. Beale, S. D. Ecklund, and R. L. Walker, Cal. Tech. Synchrotron Lab., Pasadena, California, Report No. CTSL-42, 1966 (unpublished).

¹⁹G. Buschhorn, L. Criegee, G. Franke, P. Heide, R. Kotthaus, G. Poelz, G. Vogel, U. Timm, K. Wegener, H. Werner, and W. Zimmermann, in *Proceedings of International Symposium on Electron and Photon Interactions at High Energies, 1971* [Ref. 5(b)], Paper 16.

²⁰J. Lefrancois, rapporteur's talk, International Symposium on Electron and Photon Interactions at High Energies, Cornell University, 1971 (unpublished).

²¹H. Fischer, Bonn University Report No. PI 1-122, 1970 (unpublished).

²²G. von Holtey, Bonn University Report No. PI 1-123, 1971 (unpublished).

²³H. R. Crouch, Jr., R. Hargraves, B. Kendall, R. E. Lanou, A. M. Shapiro, M. Widgoff, G. E. Fischer, C. Bordner, Jr., A. E. Brenner, M. E. Law, T. A. O'Halloran, Jr., F. D. Rudnick, K. Strauch, J. C. Street, J. J. Szymanski, P. Bastien, B. T. Feld, V. K. Fischer, I. A. Pless, A. Rogers, C. Rogers, L. Rosenson, T. L. Watts, R. K. Yamamoto, G. Calvelli, F. Gasparini, L. Guerriero, J. Massimo, G. A. Salandin, L. Ventura, C. Voci, F. Waldner, A. Brandstetter, Y. Eisenberg, A. Levy, U. Maor, and E. E. Ronat, *Phys. Rev.* **169**, 1081 (1968). See also Cambridge Bubble Chamber Group, *ibid.* **155**, 1477 (1967); **156**, 1426 (1967).